Int. J. Solids Structures, 1974, 10, pp. 361–381. Pergamon Press. Printed in Gt. Britain.

THE SUPPRESSION OF A DYNAMIC INSTABILITY OF AN ELASTIC BODY USING FEEDBACK CONTROL

CHARLES F. KALMBACH

Research Staff, Department of Aerospace and Mechanical Sciences, Princeton University, New Jersey 08540

EARL H. DOWELL

Professor, Department of Aerospace and Mechanical Sciences, Princeton University, New Jersey 08540

and

FRANCIS C. MOON

Assistant Professor, Department of Aerospace and Mechanical Sciences, Princeton University, New Jersey 08540

(*Received* 17 *May* 1973; *revised* 24 *August* 1973)

Abstract—A theoretical and experimental study is made to determine the feasibility of controlling a thin cantilevered beam subject to a (nonconservative) follower force. A theoretical model is developed using the equations for a thin beam under initial stress and Galerkin's method. An experiment is constructed with the capability of using a variety of feedback loops to control a thin aluminum beam with a tip jet mounted parallel to the chord. A particular control system is chosen for study and an increase of follower force required to destabilize the beam of over 65 per cent is recorded. The theoretical results show good correlation with the experimentally determined stability boundaries and frequency variations with follower force.

NOMENCLATURE

A	yes (1), no (0) bending sensor; also beam cross-sectional area
A_n	bending modal coefficients
$a_n = A_n/L$	
B	yes (1), no (0) torsion sensor
B_s	torsion modal coefficients
b	beam width
C	modal integrals
E	modulus of elasticity
$\mathbf{e}$	unit vector
F_s	torsion modal constants
G_n	bending modal constants
G	shear modulus
h	beam thickness
I	bending moment of inertia
J	torsion moment of inertia
K	nondimensional frequency $\equiv \left[\frac{m_B \omega^2 L^4}{EI}\right]^{1/2}$
L	beam length
$\mathbf{M}$	moment vector
M_N	nozzle mass

M_c coil mass
m_B beam density
m_T tubing density
Q control force
$\mathbf{Q}$ follower force vector
q body force
r beam radius of gyration
r_c perpendicular distance from elastic axis to control force
s Laplace Transform Variable
$\mathbf{T}$ follower moment vector
t time
u bending displacement
u_n bending natural mode
V^0 tip force
V_c feedback loop transfer function
$\mathbf{V}$ shear force vector
x, y, z coordinate system of undeformed beam
x', y', z' coordinate system of deformed beam
z_c position of control force
z_s position of sensor
$\delta(z-L)$ delta function
ε bending strain
$\gamma = \frac{GJ}{EI}$, also, torsional strain
$\lambda = \frac{V^0 L^2}{EI}$ nondimensional follower force
$\mu = \frac{T^0 L}{EI}$ nondimensional follower moment
$\lambda_c = \frac{V_c L^2 h}{EIL}$ nondimensional control force
ϕ torsional twist
ϕ_s torsion natural mode
$\rho = r/L$
$\rho_c = r_c/L$
τ body torque
ω frequency
Ω nondimensional frequency

Superscript

$\hat{}$ perturbation
$u' = \frac{\partial u}{\partial\left(\frac{z}{L}\right)}$

Subscript

F flutter
D divergence

1. INTRODUCTION

This paper presents the results of an experimental and theoretical study of a means of controlling an elastic body subject to a nonconservative force. The problem was first stated in[1]. An interim note on subsequent experimental tests was published in[2]. The research was also presented in a summary form at the XIIIth International Congress of Theoretical and Applied Mechanics in Moscow, USSR, 1972. The experiment consists of a thin cantilevered beam with an air nozzle mounted at its tip parallel to the chord line (Fig. 1).

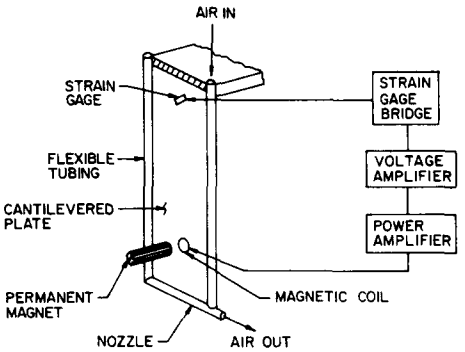

Fig. 1. Schematic of system.

Not only does the experimental model resemble a thin wing with tip jet, but it also experiences a converging frequency flutter instability similar to classical bending-torsion wing flutter. This similarity, along with the simplicity of the experiment, compared even with a wind tunnel flutter experiment, gives it a potential use as a test bed for investigating the effect of feedback control in suppressing flutter of larger, more complex systems.

Furthermore, the flexibility of the experimental set-up permits a wide range of feedback control configurations. The possibility exists, therefore, of experimentally verifying theoretical results obtained with the aid of linear feedback control, parameter optimization, and optimal feedback control theory.

The experiment, itself, is taken from the group of applied mechanics problems known as nonconservative force problems. In this regard, the study is believed to be unique for at least two reasons. First, it presents one of the first quantitative observations of this type of flutter instability in a continuous elastic system. Follower jet experiments have also been reported in[3]. Second, while previous studies have been concerned with the reduction of resonances of a system[4,5], the purpose of this study was to attempt to suppress or delay the start of an instability in a nonconservative mechanical system using feedback control.

A wide range of subjects are clearly involved in the formulation, analysis, and application of the results of this study. The second section of the first chapter of[6] surveys the major papers or books in the following areas: active flight control, flutter suppression, linear feedback control, adaptive control, parameter optimization theory, optimal feedback control theory applied to distributed and discrete parameter systems, aeroelastic optimization, and nonconservative force problems.

Briefly, motivation for this research was found in the growing number of applications of feedback control techniques to aeroelastic systems (e.g.[13,14]). Most of the studies have been directed towards a particular aerospace vehicle—the B-52[7], XB70[8], SST[9], *Space Shuttle* [10], and *Saturn* V[11] to name a few. Whether the studies were theoretical or experimental (using scale models or the real vehicle in flight test), problems arose in attempting to understand the basic effect of control on the body due to the many degrees of freedom involved. When a degree of control was achieved experimentally on a particular vehicle, it was not immediately obvious how to use that knowledge on a different vehicle.

Up to the present, most of the effort has been directed toward gust alleviation and increased fatigue life. Suppression or alleviation of flutter instability has been approached through increasing the damping of the critical modes (even if the problem is one of converging

frequency flutter). Theoretical models also suffer from the problem of size and complexity if any resemblance to the vehicle is to be maintained. If the theoretical model has been sufficiently simplified to apply analytical techniques, the problem becomes one of translating their general control requirements into specific demands.

On the other hand, simple experimental or theoretical models have often suffered from an inability to apply their results directly to full scale systems. However, Bolotin[12] and others have analyzed simple mechanical systems with nonconservative forces. Such systems potentially undergo dynamic instabilities like flutter, in addition to a static instability divergence. Furthermore, techniques of control theory can be applied to these systems in a straight forward and systematic manner with the effects on stability clearly seen (see e.g.[6,15]). Such considerations led to the present study.

In the second part of this paper the equations for a thin beam under initial stress are developed. The resulting system of partial differential equations is reduced to modal equations by Galerkin's method whose stability is assessed using root locus techniques. In the last section of that part control forces are added to the model.

The third part opens with a summary of the experimental objectives. This is followed by a description of the capabilities of the experimental apparatus and presentation of the results of the experiment. For the purposes of this study, the most important result is the system stability boundary which demonstrates the effectiveness of the control system. An increase of force required to flutter the beam of over 65 per cent is recorded. However the variation of the modal frequencies with follower force and control force are of value, as well. Subcritical, i.e. below flutter, experimental frequency variation data is seldom available in the literature. This experimental data, therefore, by itself, presents a fine opportunity for experimental–theoretical correlation.

This experimental–theoretical correlation is made in the fourth part after a discussion of the theoretical computer model. This model is based on the equations developed in the second part and corrected with experimentally obtained natural mode data. A five mode Galerkin model is seen to adequately predict the controlled and uncontrolled beam behavior. An explanation of the effectiveness of the various control configurations using the concepts of linear feedback control theory has also been formulated[6]. Appendix D of[6] elaborates on the reason for using linear control theory instead of optimal control theory in this analysis and the interested reader is referred to that source.

2. THEORETICAL FORMULATION OF THE PROBLEM

2.1 *Equation of motion for a thin beam*

The equations for a cantilevered thin beam are derived in[1] and [6]. Figure 2 displays the coordinate system used in this analysis. The undeformed body axes are x, y, and z while the deformed variables are x', y', and z'. The equations are written for a symmetric cross section, rigid in the y direction. The displacement of the neutral axis in the x direction is denoted by u while the angle of twist of the y axis about the z axis is ϕ. The angles ϕ and $\partial u/\partial z$ are considered to be small, where $\partial u/\partial z$ is the local rotation of the z axis (about the y axis).

The resultant shear force and moment on a cross section will be denoted by $\mathbf{V}$ and $\mathbf{M}$, respectively. The body force per unit length of beam is called q and the body torque is τ.

It is further assumed that in the undeformed state there exists an initial load $\mathbf{V}^0$ and $\mathbf{M}^0$.

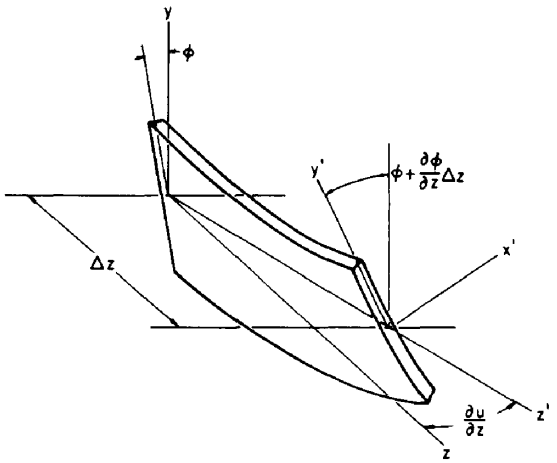

Fig. 2. Coordinate system.

Taking a small perturbation from equilibrium, one obtains three perturbation and three equilibrium equations:

$$\begin{aligned}
&\frac{\partial}{\partial z}(\hat{V}_{x'}) - \frac{\partial}{\partial z}(\phi \hat{V}_y^0) + \frac{\partial}{\partial z}\left(\frac{\partial u}{\partial z} V_z^0\right) + \hat{q}_x = 0 \\
&\frac{\partial}{\partial z}(\hat{M}_{y'}) + \frac{\partial}{\partial z}(\phi M_x^0) + \hat{V}_{x'} - \phi V_y^0 + \hat{\tau}_y = 0 \\
&\frac{\partial}{\partial z}(\hat{M}_{z'}) - \frac{\partial}{\partial z}\left(\frac{\partial u}{\partial z} M_x^0\right) + \frac{\partial u}{\partial z} V_y^0 + \hat{\tau}_z = 0
\end{aligned} \tag{1}$$

$$\frac{\partial}{\partial z}(V_y^0) + q_y^0 = 0 \qquad \frac{\partial}{\partial z}(V_z^0) + q_z^0 = 0 \qquad \frac{\partial}{\partial z}(M_x^0) - V_y^0 + \tau_x^0 = 0 \tag{2}$$

The constitutive laws as derived for a rectangular cross section, neglecting warping, are

$$\hat{M}_{y'} = EI \frac{\partial^2 u}{\partial z^2} \tag{3}$$

$$\hat{M}_{z'} = GJ \frac{\partial \phi}{\partial z}. \tag{4}$$

The inertial forces are (neglecting rotational inertia about the y axis):

$$\begin{aligned}
q_x &= -m \frac{\partial^2 u}{\partial t^2} \\
\tau_z &= -mr^2 \frac{\partial^2 \phi}{\partial t^2}.
\end{aligned} \tag{5}$$

2.2 *Addition of follower force*

The follower forces are constant with respect to the body fixed coordinates x', y', z'.

If $\mathbf{q}$ is written

$$\begin{aligned}\mathbf{q} &= Q_{x'}\mathbf{e}_{x'} + Q_{y'}\mathbf{e}_{y'} + Q_{z'}\mathbf{e}_{z'} \\ &= q_x\mathbf{e}_x + q_y\mathbf{e}_y + q_z\mathbf{e}_z\end{aligned} \tag{6}$$

then

$$q_x = Q_{x'} - \phi Q_{y'} + \frac{\partial u}{\partial z} Q_{z'}$$

$$q_y = Q_{y'} + \phi Q_{x'}$$

$$q_z = Q_{z'} - \frac{\partial u}{\partial z} Q_{x'}.$$

In particular, let

$$\mathbf{q} = Q_{y'}{}^0\,\mathbf{e}_{y'} \quad \text{and} \quad \mathbf{T} = 0. \tag{7}$$

Therefore the perturbed, $\hat{q}$, and the equilibrium, q^0, values become

$$\begin{aligned} \hat{q}_x &= -\phi Q_y^0, & q_x^0 &= 0 \\ \hat{q}_y &= 0 \quad \text{and} & q_y^0 &= Q_y^0 \\ \hat{q}_z &= 0 & q_z^0 &= 0 \end{aligned}. \tag{8}$$

Substituting (8), (3), (4) and (5) into (1), one may write

$$\begin{aligned} \frac{\partial^2}{\partial z^2}\left(EI\frac{\partial^2 u}{\partial z^2}\right) + \frac{\partial^2}{\partial z^2}(\phi M_x^0) - \frac{\partial}{\partial z}\left(V_z^0\frac{\partial u}{\partial z}\right) + m\frac{\partial^2 u}{\partial t^2} + Q_{y'}^0\phi &= q_x - \frac{\partial \tau_y}{\partial z} \\ \frac{\partial}{\partial z}\left(GJ\frac{\partial \phi}{\partial z}\right) - \frac{\partial}{\partial z}\left(M_x{}^0\frac{\partial u}{\partial z}\right) + V_y^0\frac{\partial u}{\partial z} - mr^2\frac{\partial^2 \phi}{\partial t^2} &= -\tau_z \end{aligned} \tag{9}$$

and

$$\begin{aligned} \frac{\partial M_x^0}{\partial z} - V_y^0 &= 0 \\ \frac{\partial V_y^0}{\partial z} + Q_{y'}^0 &= 0 \\ \frac{\partial V_z^0}{\partial z} &= 0 \end{aligned} \tag{10}$$

Further simplification gives (EI, GJ also assumed constant):

$$m\frac{\partial^2 u}{\partial t^2} + EI\frac{\partial^4 u}{\partial z^4} + 2V_y^0\frac{\partial \phi}{\partial z} + M_x^0\frac{\partial^2 \phi}{\partial z^2} = q_x \tag{11a}$$

$$mr^2\frac{\partial^2 \phi}{\partial t^2} - GJ\frac{\partial^2 \phi}{\partial z^2} + M_x^0\frac{\partial^2 u}{\partial z^2} = \tau_z \tag{11b}$$

and

$$\begin{aligned} \frac{\partial M_x^0}{\partial z} - V_y^0 &= 0 \\ & \qquad V_z^0 = 0. \\ \frac{\partial V_y^0}{\partial z} + Q_y^0 &= 0 \end{aligned} \tag{12}$$

Boundary conditions for this case are

$$M_y = M_z = V_x = V_z = 0 \quad \text{at} \quad z = L$$

the first two of which give (from (3) and (4))

$$\frac{\partial^2 u}{\partial z^2} = \frac{\partial \phi}{\partial z} = 0 \qquad z = L \tag{13a}$$

and the third from (1b) and (3)

$$V_x = \phi V_y^0 - \frac{\partial}{\partial z}(\phi M_x^0) - \frac{\partial}{\partial z}\left(EI \frac{\partial^2 u}{\partial z^2}\right) = 0$$

or using (10a)

$$-EI \frac{\partial^3 u}{\partial z^3} - M_x^0 \frac{\partial \phi}{\partial z} = 0 \qquad z = L. \tag{13b}$$

Condition (13b) can be simplified using (13a) to

$$\frac{\partial^3 u}{\partial z^3} = 0.$$

Conditions at the clamped end are

$$u = \frac{\partial u}{\partial z} = \phi = 0 \qquad z = 0. \tag{14}$$

2.3 *Addition of follower moment*

Follower moments may also be applied to the beam. Analysis of this problem is given in[6].

2.4 *Reduction to modal equations*

Using Galerkin's method, we will reduce to ordinary differential equations the partial differential equations (11).

We call u_m and ϕ_r the natural modes in bending and torsion of a clamped-free beam and assume

$$\begin{aligned} u &= \sum_m A_m u_m(z) \\ \phi &= \sum_r B_r \phi_r(z). \end{aligned} \tag{15}$$

The functions u_m and ϕ_r satisfy the boundary conditions (13) and (14) as well as the following differential equations (non-dimensionalized with $' \equiv \partial/\partial(z/L)$ in which G_m and F_r are known constants

$$\begin{aligned} u_m'''' - G_m{}^4 u_m &= 0 \\ \phi_r'' + F_r{}^2 \phi_r &= 0. \end{aligned} \tag{16}$$

In addition, the following orthogonality conditions are met:

$$\begin{aligned} \int_0^L u_m u_n \, dz &= \delta_{mn} \\ \int_0^L \phi_r \phi_s \, dz &= \tfrac{1}{2} \delta_{mn}. \end{aligned} \tag{17}$$

The following equations are obtained after substituting (15) into (11), observing (16), multiplying (11a) by u_n and (11b) by ϕ_s, and finally integrating over z.

$$\left(m\frac{\partial^2 A_n}{\partial t^2} + EIG_n^4 A_n\right)\int_0^L u_n^2\frac{dz}{L} + \frac{2}{L}\sum_r B_r\int_0^L V_y^0\,\phi_r' u_n\frac{dz}{L}$$
$$+\frac{1}{L^2}\sum_r B_r\int_0^L M_x^0\,\phi_r'' u_n\frac{dz}{L} = \int_0^L q_x u_n\frac{dz}{L} \tag{18}$$
$$\left(mr^2\frac{d^2B_s}{dt^2} + \frac{GJ}{L^2}F_s^2 B_s\right)\int_0^L \phi_s^2\frac{dz}{L} + \frac{1}{L^2}\sum_m A_m\int_0^L M_x^0\,u_m''\,\phi_s\frac{dz}{L} = \int_0^L \tau_z\phi_s\frac{dz}{L}.$$

Equations (18) are valid for an arbitrary distribution of follower forces. We now specialize to the case investigated in the rest of this study. In the case of a jet of air located at the tip to provide the follower force,

$$Q_{y'}^0 = V^0\,\delta(z-L). \tag{19}$$

Thus from (10)

$$\begin{aligned} V_y^0 &= V^0 \\ M_x^0 &= V^0(z-L). \end{aligned} \tag{20}$$

Substituting these equations into (18) and non-dimensionalizing (see Nomenclature), one obtains:

$$\left(\frac{d^2a_n}{d\tau^2} + K_n^2\,a_n\right)C1_{nn} + \lambda\sum_r B_r C8_{rn} = \frac{L^3}{EI}\int_0^L q_x u_n\frac{dz}{L}$$
$$\left(\frac{d^2B_s}{d\tau^2} + \Omega_s^2\,B_s\right)C2_{ss} + \frac{\lambda}{\rho^2}\sum_m a_m C9_{sm} = \frac{1}{\rho^2}\frac{L^2}{EI}\int_0^L \tau_z\phi_s\frac{dz}{L}. \tag{21}$$

2.5 *Specification of control force*

We specify the control force Q_i to be proportional to the bending and/or torsion strain at some point $z_i = z_{s_i}$. It is applied at location $z_i = z_{c_i}$ and $y_i = r_{ci} = L\rho_{ci}$. If V_c is the transfer function of the feedback loop, then

$$Q_i = V_c(A\varepsilon(z_{s_i}) + B\gamma(z_{s_i})). \tag{22}$$

where A and B can be ± 1 or 0 indicating that bending and torsion strain is or is not being sensed, and where

$$\begin{aligned} \gamma(z_s) &\equiv \frac{h}{L}\phi'(z_s) \\ \varepsilon(z_s) &\equiv \frac{h}{L}u''(z_s). \end{aligned} \tag{23}$$

Equation (23) assumes the use of two additive strain gages. With the above definitions,

$$\begin{aligned} q_x &= \sum_i Q_i\,\delta(z-z_{ci}) \\ \tau_z &= -\sum_i r_{c_i} Q_i\,\delta(z-z_{ci}). \end{aligned} \tag{24}$$

The right-hand side of equations (21) can now be written in non-dimensional form as

$$\frac{L^3}{EI}\int_0^1 q_x u_n \frac{dz}{L} = \sum_i u_n(z_{c_i})\lambda_{c_i} B \sum_r \left(B_r \phi_r'(z_{s_i}) + A \sum_m a_m u_m''(z_{s_i})\right)$$
$$\frac{L^3}{\rho^2 EI}\int_0^1 \tau_z \phi_s \frac{dz}{L} = -\sum_i \phi_s(z_{c_i})\rho_{c_i}\frac{\lambda_{c_i}}{\rho^2}\left(B\sum_r B_r \phi_r'(z_{s_i}) + A\sum_m a_m u_m''(z_{s_i})\right). \tag{25}$$

The feedback loop is specialized to the case of one sensor and one control force application point. The feedback loop transfer function is considered to be a pure gain and to represent force applied by the control force per unit strain detected by the sensor.

Equation (21) is now a system of ordinary differential equations for $A_m(=La_m)$ and B_r, the coefficients of the natural modes defined in (15).

3. EXPERIMENTAL STUDIES

3.1 *Experimental objectives*

An extensive experimental program was initiated to verify the results of the theoretical analysis and to demonstrate on an actual elastic body the techniques of control proposed in this paper.

The specific configuration studied is a vertical, cantilevered, thin aluminum beam with an air jet mounted at its free end parallel to its width (see Fig. 1). The follower force is then proportional to the square of the jet velocity. The feedback loop sensors are strain gages mounted on the beam. The control forces are provided by wire coils mounted on the beam which, when supplied with a current proportional to the output of the strain gages, create a magnetic field that interacts with the field of externally supported permanent magnets.

As stated above,[1] reported quantitative results of the experimental suppression of an instability with feedback. It was a conclusion of that paper that "the flutter instability of a beam under a transverse follower force (without feedback control) is well understood on experimental and physical grounds".

However, the omission of a term in the nondimensional form of the control equation presented in[1] (due to an algebraic error) resulted in the prediction of an incorrect stability boundary. This also promoted a pessimistic view of the value of pure gain compensation in the feedback loop and hence the recommendation to introduce dynamics into the feedback loop.

The addition of this missing term to the analysis indicated that substantial suppression of flutter could be acieved using only gain compensation. Since the main objective is to demonstrate the feasibility of suppressing dynamic instabilities, the feedback loop has been kept as simple as possible, leaving other forms of compensation to future research.

As in most experimental studies, there was a great deal of interaction between the experiment and the developing theoretical model. In particular, the theoretical model needed three types of experimental data as inputs or as checks on its predictions: natural frequencies of beam vibration, variation of these frequencies with follower force, and the shape of the natural modes. This data is discussed and presented in sections 3.4.2–3.4.4 of[6].

The most important experimental result is the stability boundary. The improvement in this boundary through feedback control, the single most significant result of this research, is discussed in section 3.4.

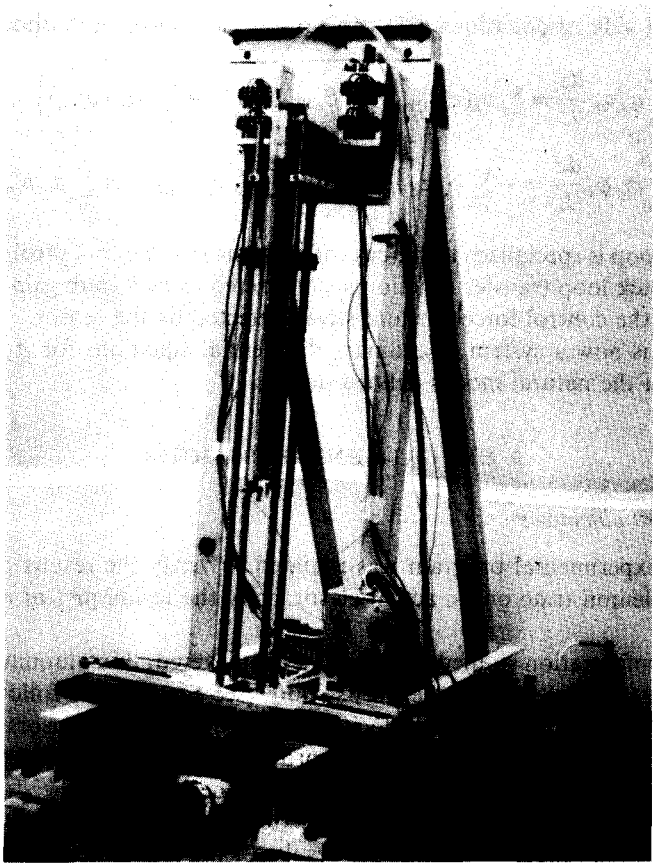

Fig. 3. General view of equipment.

3.2 *Test facility*

The experimental apparatus (Fig. 3) was built over a steel plate welded to a pair of U channels. 1/2 in. aluminum angle provides vertical and lateral support. Up to 3 in. of the beam specimen is held clamped between 1/2 in. aluminum plates (Fig. 4). The magnets are mounted in phenolic blocks (see Fig. 5) which clamp around 3/8 in. steel ready rod. The rods are held at both ends by plates of aluminum which are free to travel back and forth in tracks. The bottom track mounted on a phenolic base employs threaded rods for accurate lateral placement. Once in place, the rods are quickly fixed with the aid of cap screws in both the top and bottom supports.

In order to eliminate as much of the initial beam deformation as possible, care was taken to select and prepare as flat a specimen as possible. Table 1 notes the dimensions of the beam. After some experimenting, it was decided to attach the plastic tubing to the sides of the beam with a continuous strip or tape (see Fig. 4). This procedure seemed to eliminate much of the distortion in the tubing. Both bending and torsion sets of strain gages are semi-conductor.

Finally, a method was devised to easily relocate the control force. As seen in Fig. 5 the coils are mounted on plastic bases with holes in the center. At every 2 in. along the beam length (or 10 per cent of the total length) a pair of holes have been drilled to allow passage

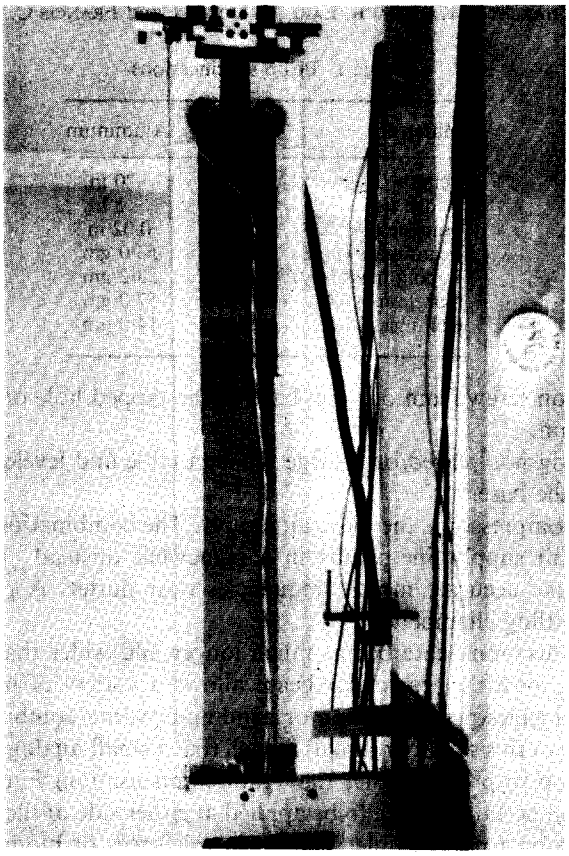

Fig. 4. Side view of beam.

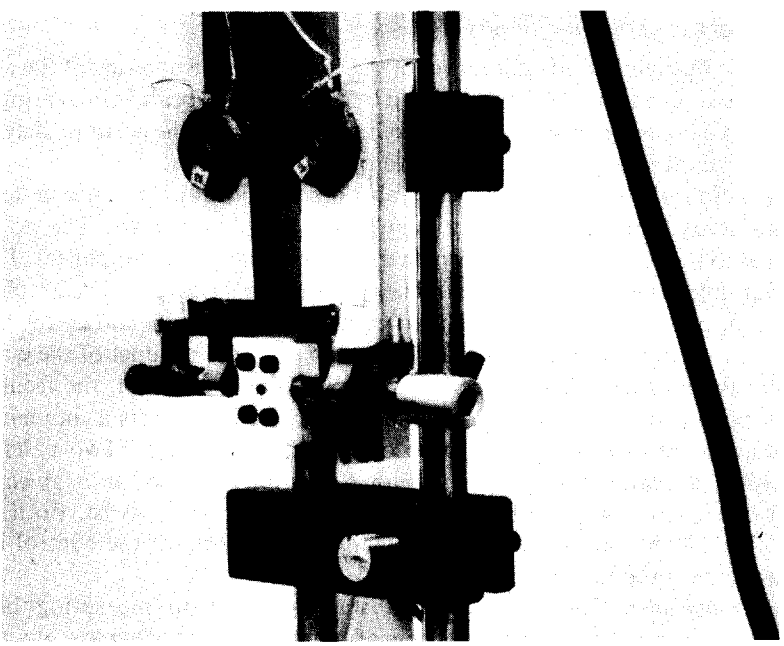

Fig. 5. Lower beam with coil, nozzle, and magnet holder.

Table 1. Beam specifications

Material	Aluminum
Length L	20 in.
Width b	3 in.
Thickness h	0.02 in.
Beam mass ($m_B L$)	53·0 gm
Tubing mass ($m_T L$)	53·2 gm
Nozzle mass M_N	57·0 gm
Coil mass (4 coils) M_c	14·0 gm

of a machined nylon screw from one coil base to the tapped hole of the base on the opposite side of the beam.

This entire test rig was placed on a large wooden table and leveled by means of a screw in each corner of the base.

A Schraum air compressor is the basic air supply. The combination of many valves along with an extended air supply line results in a somewhat unsteady flow. It is particularly difficult to determine accurate modal frequencies near flutter. A possible solution is the installation of a settling chamber.

The test rig can accommodate beams much longer and wider than the one described in Table 1. However, even this particular beam allows a variety of interesting experiments. Two pairs of strain gages permit torsion or bending or some combination of signal to be sensed. The quality of this signal or signals is such that a small analog computer can be used in the feedback loop to provide other than gain compensation. Finally, two pairs of coils at each body station permits a force to be applied at either side of the $y' = 0$ axis as well as a pure bending force or a pure couple. These control forces or moments can be applied at several stations to represent a distributed control.

3.3 *Preliminary experimental results*

Calibration. The method of calibration of the follower force in terms of the air pressure is given in[6]. As shown there, the force exerted by the jet on the beam is increasingly nonlinear with respect to increasing pressure in the feed lines. This makes the accurate determination of frequency variation with jet force difficult to obtain near flutter.

The calibration of the feedback force is also described in[6]. The specific feedback loop used in this study employs only the torsion strain gages as sensors. The voltage directly proportional to the torsion strain is amplified by signal and power amplifiers. The amplifiers exhibit a flat, linear response over the frequency range of 0–100 cps. The amplified signal is fed to one pair of coils on the beam. The force exerted on the wire coil by the radial field of the permanent, stationary magnet is proportional to the cross product of the current though the coil and the magnetic field. Since the magnetic field is constant, the feedback force is linearly proportional to the current. (The magnetic field also exerts a moment on the coil which is considered in this analysis to be of second importance.) Two pairs of coils are always used at a station for symmetry. Either pair may be used in a given experiment. This form of control results in both a bending deflection and a twist. Both positive and negative values of the gain are available. Finally, the location of the control input station may be varied over the range $0{\cdot}1 \leq z_c/L \leq 0{\cdot}95$.

Natural Frequencies. Considerable effort was expended in measuring beam natural frequencies, i.e. with no jet force. The effects of tubing mass, nozzle mass, etc. as well as the

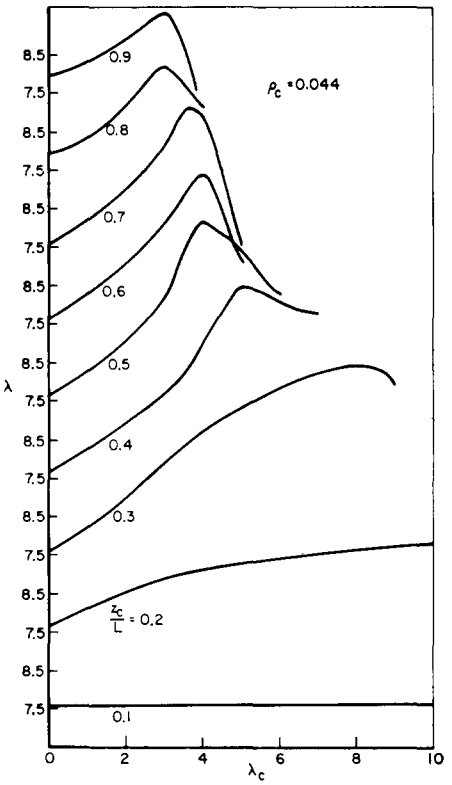

Fig. 6. Follower force vs control force (stability boundary).

effect of control force were studied. For the sake of brevity, the reader is referred to[6] for these interesting results.

3.4 *Stability boundaries*

The nondimensional jet and control forces λ and λ_c have been previously defined. A stability boundary for the system can be obtained by noting the first unstable values of λ (λ_F) for each λ_c available. It is with the aid of λ vs λ_c stability curves that the merit of a control system configuration can be determined. Figure 6, is a survey of the stability boundaries for all control input stations along the beam. The system is stable for values of λ and λ_c below the curves. Since all stations experience flutter at approximately the same follower force λ for $\lambda_c = 0$, on Fig. 6 each station is separated along the vertical axis.

These curves are positive ρ_c, which means that the pair of coils at $y' > 0$ were used. For this sign of ρ_c, positive λ_c is the stabilizing sign of the feedback for all stations. Negative λ_c results in flutter for λ below that obtained for $\lambda_c = 0$ for all stations.

Looking first at the extreme stations, one observes that the control has almost no effect at $z_c/L = 0{\cdot}1$. This is reasonable since the displacements of the modes are very small at this point. The modal displacements are the greatest at the tip but it is clear that flutter is not suppressed the most there. The maximum value of λ was obtained at $z_c/L = 0{\cdot}3.$–0.5.

At $z_c/L = 0{\cdot}9$ one also observes that the curve is composed of two types of instabilities (Fig. 7). From negative λ_c through $\lambda_c = 3$, the curve represents the stability boundary for

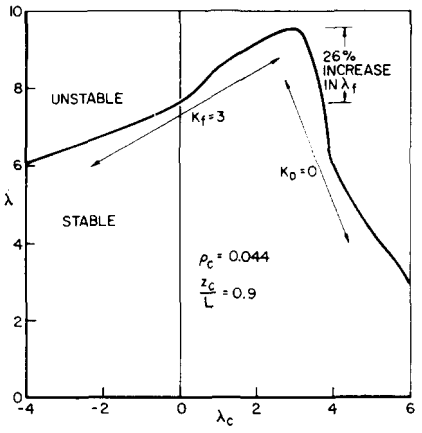

Fig. 7. Follower force vs control force (stability boundary).

converging frequency flutter. Beyond $\lambda_c = 3$ another type of instability takes over. Physically, at this point it is impossible to hold the beam centered between the externally supported permanent magnets. It seems as if the first bending mode is diverging.

This divergence-like phenomena takes place at higher λ and λ_c as the coils are moved up the beam. Between $z_c/L = 0{\cdot}9$ and $0{\cdot}6$ it seems, therefore, that the maximum value of λ obtainable is a function of λ_c and z_c/L. However, between $z_c/L = 0{\cdot}5$ and $0{\cdot}3$, a divergence occurs at a constant jet force, $\lambda = 12{\cdot}5$. This instability does not seem to be a very strong function of the control system. This is seen more clearly on Fig. 8 discussed later.

In order to determine more accurately the nature of the stability boundaries, two stations were selected for more detailed study. $z_c/L = 0{\cdot}9$ was chosen because it represents the best

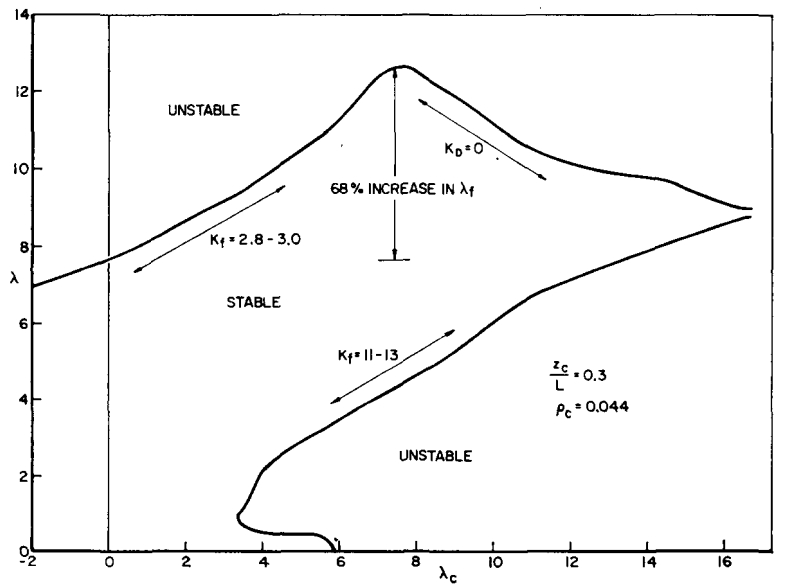

Fig. 8. Follower force vs control force (stability boundary).

intuitive choice for control placement. $z_c/L = 0{\cdot}3$ was chosen because at this station the greatest stable variation of λ_c at high λ was recorded.

Figure 7 presents the λ vs λ_c curve for $z_c/L = 0{\cdot}9$. All combinations of λ and λ_c under the curve are stable conditions. The two previously described parts of the stability curve are now clearly defined. The converging frequency flutter instability (whose frequency $K_f = 3{\cdot}0$) changes at $\lambda_c = 3$ to a bending divergence ($K_D = 0$) with steep negative slope. At the peak, however, the force needed to flutter the beam is increased by 26 per cent over the uncontrolled case.

Figure 8, representing the stability curve at $z_c/L = 0{\cdot}3$, show a more involved boundary than occurred at $z_c/L = 0{\cdot}9$. Combinations of λ and λ_c within the curve are stable configurations. This boundary now has three clearly defined regions. The portion between low negative values of λ_c and $\lambda_c = 7$ consists of the converging frequency flutter instability The region between $\lambda_c = 7$ and 17 represents a bending divergence (zero frequency) of a different nature than observed in the $z_c/L = 0{\cdot}9$ case. The main difference is the far more moderate slope. The final region of the boundary consists of a torsional oscillation of higher frequency than the above flutter.

In summary, the two stability curves for $z_c/L = 0{\cdot}9$ and $0{\cdot}3$ are representative of the curves for the stations in the two regions divided by $z_c/L = 0{\cdot}5$. As one raises the control station from $z_c/L = 0{\cdot}9$ one can see that the maximum point of the boundary increases in both the λ and λ_c directions. At approximately $z_c/L = 0{\cdot}5$ a "lid" seems to be placed on the rise of the boundary. This creates a relatively flat portion of the boundary until the third region intersects the main curve. Beyond $z_c/L = 0{\cdot}3$, the boundary flattens out indicating little stability increase with control. The maximum increase in flutter force of 67 per cent was recorded at stations $z_c/L = 0{\cdot}3$ –$0{\cdot}5$.

4. CORRELATION OF THEORY AND EXPERIMENT

Part 2 develops the equations of motion for a thin cantilevered beam with follower force. The use of Galerkin's method reduces the coupled, nonconstant coefficient, partial differential equations (11a, b) to equations (21) and (25) which represent a system of linear, coupled, constant coefficient differential equations in the coefficients a_i and B_i of the Galerkin modes. The particular Galerkin modes used are the natural bending and torsion modes of a cantilevered beam. These modes are the exact solution to equations (11a, b) when there is no follower force and no control force. The effect of the follower force was experimentally observed to couple together these natural modes so that each beam mode at a non-zero follower force appears to be a sum of the natural modes. Analysis of the system of equations (21) and (25) will demonstrate this, as well. This system represents a set of linear, homogeneous. ordinary differential equations which can be reduced to linear algebraic equations by a Laplace transformation with respect to time. Solving the characteristic equation of this set of linear algebraic equations produces a set of roots or eigenvalues which can be interpreted as frequencies of the beam modes of vibration. Each eigenvalue can then be substituted back into the characteristic determinant to find the associated eigenvector. These eigenvectors can be interpreted as the relative weights of each natural mode in the particular beam motion at any given operating condition, i.e. combination of follower and control forces. The number of assumed natural modes necessary to adequately represent the real beam is discussed in 4.1.

The nature of the physical problem can be most easily visualized with the use of three natural modes: first and second bending and first torsion. The characteristic equation for

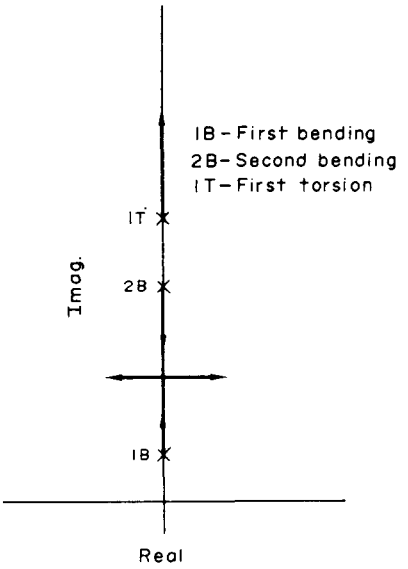

Fig. 9. Root locus schematic.

this system is a polynominal of sixth order in the Laplace transform variable s. When the control force λ_c is zero, the nondimensional follower force λ appears in this equation linearly in λ^2. The characteristic equation can therefore be placed in the standard root locus form with λ^2 as the gain and $Q(s)$ and $P(s)$ polynominals in s:

$$1 + \lambda^2 \frac{P(s)}{Q(s)} = 0.$$

One can then observe the effect on the eigenvalues of the follower force by constructing the root locus. The locus starts at the system poles, denoted by x in Fig. 9 and found by setting $Q(s) = 0$. These poles are the frequencies of the natural modes. It is observed that the follower force couples the natural modes and changes the modal frequencies as shown in Fig. 9 (for zero control force). The frequencies of the first two modes are driven together. At the point of coalescence one root acquires a positive real part and the other acquires a negative real part. The positive real part indicates a flutter instability. The object of the control is to delay the convergence of these roots and so to increase the follower force needed to flutter the beam.

4.1 *Computer model*

The computer programs used in the research are described in[6]. Comparison of results using different numbers of modes over a variety of beam configurations dictated the use of five modes in the final analysis. The modes are the first three bending and first two torsion modes.

The equations for the beam were written for uniform mass and stiffness. The presence of the added masses due to the coils, tubing and nozzle required correction of the modal integrals and resulted in a non-diagonal mass matrix for certain configurations. Non-ideal

stiffness characteristics were also taken into account by using experimentally determined modal frequencies.

In addition to corrections for nonuniform mass distribution, other corrections could be made for the presence of structural damping, gravity, the "garden hose effect," and the oscillation due to fluctuations in the air delivery line. Discussion of these latter effects is presented in[6].

4.2 *Theoretical results and correlation with experimental data*

In this section theoretical results are compared with the experimental observations of part 3. The close agreement between the model predictions and actual observations increases our confidence in our ability to undetstand the manner in which the application of control affects the system stability boundary.

4.2.1 *Frequency Variation with Follower and Control Force.* Figures 10 and 11 show the predicted and observed variation of frequency with follower force $z_c/L = 0{\cdot}9$ and $0{\cdot}3$. Experimental–theoretical correlation is generally good except when $\lambda > 7$. The worst correlation is at the onset of flutter where the observed flutter frequency is measurably lower than the predicted value.

4.2.2 *Mode Shapes.* Figure 12 is a theoretical check on the observed node lines of the beam. The node lines were calculated using the roots of the system characteristic equation for each λ. Each root, when substituted back into the characteristic equation, produced an eigenvector. The components of this eigenvector were then multiplied by the amplitude at each longitudinal station of each of the first three independent modes. This produced a bending deflection and twist at each longitudinal station for this particular mode, and the node lines indentified (see Fig. 12).

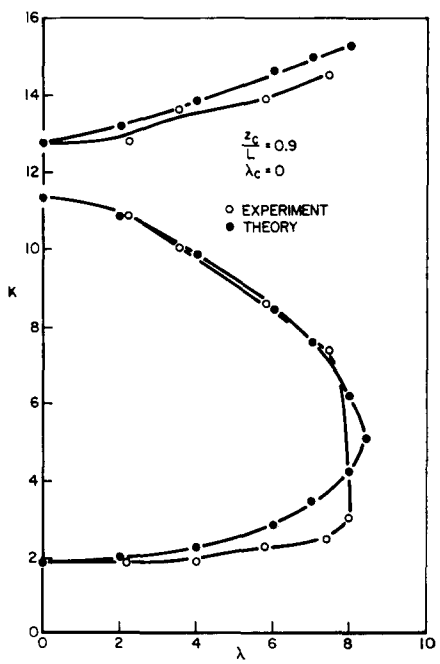

Fig. 10. Frequency vs follower force.

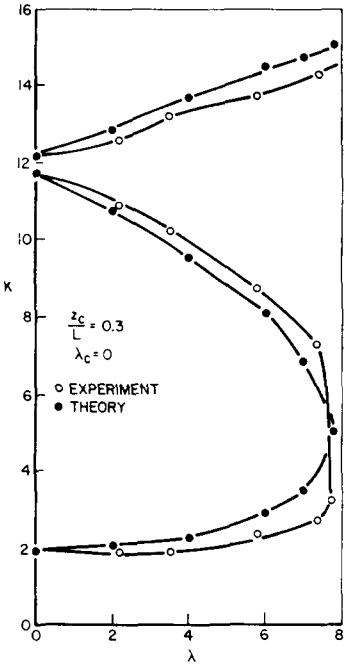

Fig. 11. Frequency vs follower force.

The predicted node lines are very close to the observed ones. The portion of the node lines at small z/L were hard to observe due to the small beam deflections in this region.

4.2.3 *Stability Boundaries.* Figures 13 and 14 show the experimentally and theoretically derived stability boundaries for $z_c/L = 0{\cdot}9$ and $0{\cdot}3$, respectively. The experimental error is

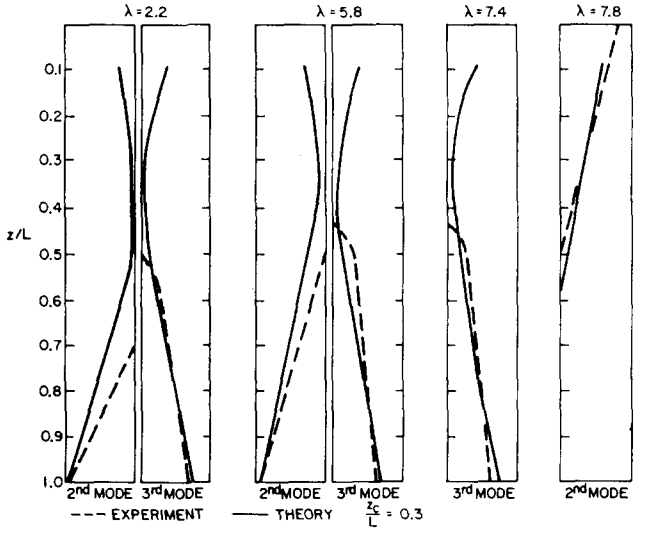

Fig. 12. Beam node lines $\lambda_c = 0$.

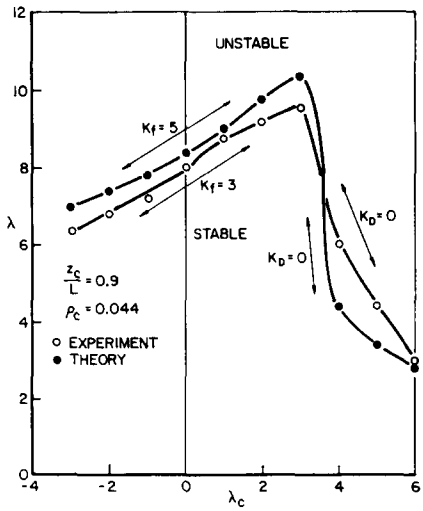

Fig. 13. Follower force vs control force (stability boundary).

different for each region of the stability boundary. The upper region is found by raising λ for a given λ_c. This gives an accuracy of $\Delta\lambda = \pm 0{\cdot}4$ (or a feedline pressure of $\pm 0{\cdot}5$ psi). The lower region of the curve is found by increasing λ_c for a fixed value of λ. This gives an accuracy of $\lambda_c = \pm 0{\cdot}5$.

The theoretical–experimental correlation at the two representative control input stations is quite good. As seen in Fig. 13, the model predicts the correct nature of the stability boundary as a function of λ_c for $z_c/L = 0{\cdot}9$. The model shows quite clearly what happens along the

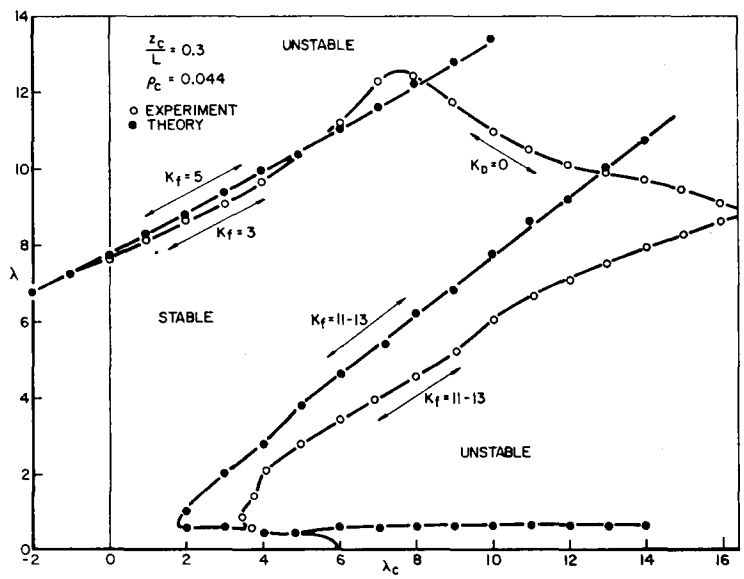

Fig. 14. Follower force vs control force (stability boundary).

divergence portion of the boundary. For any $\lambda_c > 0$ the effect of λ is to first decrease and then increase the frequency of the first beam mode. As λ_c increases, the minimum frequency reached by the first mode decreases. Finally at $\lambda_c = 3$, the first beam mode frequency reaches the real axis and divergence occurs. Increasing λ_c beyond this point decreases the jet force necessary to force the first mode to diverge.

Figure 14 shows that excellent predicted–observed agreement exists in the low frequency flutter boundary for $z_c/L = 0{\cdot}3$. The correlation is not as good along the higher frequency flutter region, but the experimental error is greater in this area. Also correlation is not good along the divergence boundary in Fig. 14.

5. CONCLUSIONS

The main objective of this study has been accomplished. The control of a particular dynamic instability of an elastic body has been demonstrated. Suppression of the converging frequency flutter for an increase of follower force of over 65 per cent has been recorded with a relatively simple feedback system. The simplicity of the feedback loop increases the possibility of extending this work to larger systems, in particular flexible aerodynamic surfaces.

Furthermore, the behavior of the beam subjected to a follower force with and without control has been accurately modelled with a finite mode Galerkin approach. The coupling effect of the follower force has been observed and an approach to understanding the effect of feedback control has been proposed[6]. This approach seeks to understand the control of the beam modes by recognizing them to be the coupled sums of the normal bending and torsion modes. This is important when not only increased stability at a specific operating point but also the maximum increase of the stable region is desired.

As discussed in[6], methods of optimal feedback control are not readily applicable to this type of problem, particularly when experimental–theoretical correlation is desired. However, the important role of parameter optimization methods during the theoretical formulation of a problem has been documented once again.

The experimental set up is satisfactory and versatile. The similarity between the flutter exhibited by the beam with transverse follower force and the classic torsion-bending flutter of an aircraft wing gives this experiment good potential as a test bed for techniques of flutter control. However, the experimental demonstration of suppression of a dynamic instability in an elastic body is of interest, by itself.

REFERENCES

1. F. C. Moon and E. H. Dowell, The control of flutter instability in a continuous elastic system using feedback. Presented at *AIAA/ASME 11th Structures, Structural Dynamic, and Materials Conference*, April (1970).
2. C. F. Kalmbach, Feedback control of flutter instability in a continuous elastic system. *AIAA Journal*, **10**, May (1972).
3. S. N. Prasad and G. Herrmann, Stability of a cantilevered bar subjected to a transverse follower force of fluid jet. *Sonderabdruck aus Ingenieur-Archiv*. **39**, Band **5** 1970.
4. A. S. Knyazev and B. D. Tartakovskii, Application of electromechanical feedback for the damping of flexural vibrations in rods. *Soviet Physics–Acoustics*, **11**, 150–154, October–December (1965).
5. A. S. Knyazev and B. D. Tartakovskii, Vibrational frequency characteristics of bars constrained by electromechanical feedback. *Soviet Physics–Acoustics*, **12**, 36–41, July–September (1966).
6. C. F. Kalmbach, Active control of an elastic body. Ph.D. Thesis Princeton University, also Department of Aerospace and Mechanical Sciences Report 1036-T, May (1972).
7. G. E. Hodges, Active flutter suppression—B52 controls configured vehicle. AIAA Dynamics Specialist Conference, Williamsburg, Va., March (1973).
8. J. H. Wykes, L. U. Nardi and A. S. Mori, XB–70 structural mode control system design and performance analyses. NASA CR-1557, July (1970).

9. Supersonic transport moving base simulation controllability test results and criteria development. The Boeing Company Report D3-7600-14, December (1969).
10. R. H. Larsen and J. H. Wykes, Assessment of the potential for load alleviation concepts for space shuttle vehicles. North American Rockwell Corporation (1970).
11. D. E. Johnston and W. A. Johnson, Feasibility of conventional control techniques for large highly coupled elastic boost vehicles. Systems Technology, Inc. California, NASA CR-88760, 1967.
12. V. V. Bolotin, *Nonconservative Problems of the Theory of Elastic Stability*. Pergamon Press (1963).
13. J. G. Theisen and N. C. Robinette, Servo control of flutter. Volume of Technical Papers on Structural Dynamics of the AIAA Structural Dynamics and Aeroelasticity Specialist Conference, p. 228, New Orleans, April (1969).
14. E. Nissim, Suppression of flutter—patent application. Filed 25 March (1971), p. 29 (NASA-Case-LAR-1082).
15. T. M. Yang and G. Herrmann, Feedback control of circulatory elastic systems. Stanford University Report SUDAM Report No. 72-7, May (1972).

Абстракт — Предполагается теоретическое и экспериментальное исследование, с целью определения возможности регулирования тонкой, консольной балки, подверженной действию неконсервативной, следящей силы. Определяется теоретическая модель путем применения уравнений тонкой балки, под влиянием начальных напряжений и метода Галеркина. Строится эксперимент, который дает возможность применить разнообразие петлей обратной связи, с целью регулировки тонкой алюминиевой балки, с концевой струей прикрепленной параллельно к хорде. Избирается частная система регулирования для исследования явления. Регистрируется прирост следящей силы, необходимой для дестабилизации балки, выше 65%. Теоретические результаты указывают надлежащее согласование с определенными экспериментально пределами устойчивости и изменениями частоты, в зависимости от следящей силы.